J Neurophysiol 112: 1703–1713, 2014.
First published July 2, 2014; doi:10.1152/jn.00854.2013.

Excitatory and inhibitory synaptic connectivity to layer V fast-spiking interneurons in the freeze lesion model of cortical microgyria

Xiaoming Jin,[1,2,4] Kewen Jiang,[1,3] and David A. Prince[4]

[1]*Stark Neurosciences Research Institute, Indiana Spinal Cord and Brain Injury Research Group, Indiana University School of Medicine, Indianapolis, Indiana;* [2]*Departments of Anatomy and Cell Biology, Indiana University School of Medicine, Indianapolis, Indiana;* [3]*Department of Neurology, Children's Hospital of the Zhejiang University School of Medicine, Hangzhou, Zhejiang, China; and* [4]*Department of Neurology and Neurological Sciences, Stanford University School of Medicine, Stanford, California*

Submitted 4 December 2013; accepted in final form 1 July 2014

Jin X, Jiang K, Prince DA. Excitatory and inhibitory synaptic connectivity to layer V fast-spiking interneurons in the freeze lesion model of cortical microgyria. *J Neurophysiol* 112: 1703–1713, 2014. First published July 2, 2014; doi:10.1152/jn.00854.2013.—A variety of major developmental cortical malformations are closely associated with clinically intractable epilepsy. Pathophysiological aspects of one such disorder, human polymicrogyria, can be modeled by making neocortical freeze lesions (FL) in neonatal rodents, resulting in the formation of microgyri. Previous studies showed enhanced excitatory and inhibitory synaptic transmission and connectivity in cortical layer V pyramidal neurons in the paramicrogyral cortex. In young adult transgenic mice that express green fluorescent protein (GFP) specifically in parvalbumin positive fast-spiking (FS) interneurons, we used laser scanning photostimulation (LSPS) of caged glutamate to map excitatory and inhibitory synaptic connectivity onto FS interneurons in layer V of paramicrogyral cortex in control and FL groups. The proportion of uncaging sites from which excitatory postsynaptic currents (EPSCs) could be evoked (hotspot ratio) increased slightly but significantly in FS cells of the FL vs. control cortex, while the mean amplitude of LSPS-evoked EPSCs at hotspots did not change. In contrast, the hotspot ratio of inhibitory postsynaptic currents (IPSCs) was significantly decreased in FS neurons of the FL cortex. These alterations in synaptic inputs onto FS interneurons may result in an enhanced inhibitory output. We conclude that alterations in synaptic connectivity to cortical layer V FS interneurons do not contribute to hyperexcitability of the FL model. Instead, the enhanced inhibitory output from these neurons may partially offset an earlier demonstrated increase in synaptic excitation of pyramidal cells and thereby maintain a relative balance between excitation and inhibition in the affected cortical circuitry.

epilepsy; neocortex; electrophysiology; caged glutamate; microgyria

DISORDERS OF NEOCORTICAL DEVELOPMENT resulting from disrupted neurogenesis, migration, or differentiation are characterized by abnormal cortical cytoarchitecture, with altered positioning and morphology of neurons (Taylor et al. 1971; Palmini et al. 2004), and are often associated with a number of clinical disorders such as mental retardation, cognitive deficits, and frequently with intractable epilepsy (Guerrini et al. 1999; Roper and Yachnis 2002). Polymicrogyria is a type of cortical malformation characterized by multiple small gyri macroscopically and four-layered cortex without deep layers microscopically (McBride and Kemper 1982; Barth 1987). The incidence of epilepsy in this condition is estimated to be as high as 87% (Barkovich and Kjos 1992; Gropman et al. 1997; Guerrini and Filippi 2005). Prenatal traumatic events, infection, and hypoxia between the 20th and 24th wk of gestation are believed to cause cell death and lead to the formation of polymicrogyria (Barkovich and Lindan 1994; Barkovich et al. 1995; Montenegro et al. 2002). Genetic abnormalities as a mechanism underlying human polymicrogyria have also been described (Piao et al. 2004).

The transcortical freeze lesion (FL), created by briefly contacting the exposed skull of neonatal rats or mice with a freezing probe, provides a rodent model of cortical microgyria that histologically mimics human four-layered polymicrogyria (Dvorak and Feit 1977; Jacobs et al. 1996; Redecker et al. 2005). Although the FL rats may not develop spontaneous seizures (Kellinghaus et al. 2007), they exhibit a decreased seizure threshold for hyperthermia-induced seizures in vivo (Scantlebury et al. 2004), and their brain slices generate epileptiform activity in the paramicrogyral (PMG) region in vitro (Jacobs et al. 1996, 1999; Luhmann et al. 1998). Studies in this model have shown abnormal induction of neocortical long-term potentiation (Peters et al. 2004), widespread downregulation of the expression of gamma-aminobutyric acid type A ($GABA_A$) receptor subunits within the cortical malformation and remote brain regions (Redecker et al. 2000), and an increase in binding to *N*-methyl-D-aspartate (NMDA), 2-amino-3-(3-hydroxy-5-methyl-isoxazol-4-yl) propanoic acid (AMPA), and kainate receptors and a reduction of binding to $GABA_A$ and $GABA_B$ receptors in the malformed neocortex (Zilles et al. 1998). Excitatory synaptic transmission is enhanced in layer V pyramidal neurons of the PMG region (Jacobs and Prince 2004), likely resulting from enhanced synaptic connectivity and glutamate release from both superficial and deep layers (Brill and Huguenard 2010; Dulla et al. 2012). Interestingly, inhibitory synaptic transmission is also enhanced, which is mainly driven by network activity (Prince et al. 1997; Jacobs et al. 1999) and increased strength of inhibitory synapses (Brill and Huguenard 2010). However, it is unclear how changes in the inhibitory circuits in the PMG region may contribute to the observed increase of inhibition in the cortical pyramidal neurons.

Fast-spiking (FS) interneurons belong to the largest class of inhibitory cells in the cortex (Uematsu et al. 2008). By making GABAergic synapses on the somata and proximal dendrites of cortical pyramidal neurons (DeFelipe 1997; Freund and Katona

Address for reprint requests and other correspondence: D. A. Prince, Neurology and Neurological Sciences, Stanford Univ. School of Medicine, Rm. M016, Stanford, CA 94305-5122 (e-mail: daprince@stanford.edu).

2007), they play critical physiological roles in controlling the action potential (AP) firing and filtering of excitatory inputs onto pyramidal neurons within cortical circuits. To better understand synaptic connectivity to cortical interneurons in paramicrogyral cortex, we used laser scanning photostimulation (LSPS) and whole cell patch-clamp recording techniques (Jin et al. 2006, 2011) to map excitatory and inhibitory input onto the FS interneurons in the FL and homotopic control cortex in a line of transgenic mice that specifically expressed green fluorescent protein (GFP) in these neurons. Results of LSPS mapping showed that excitatory synaptic connections were increased and inhibitory inputs were decreased in FS interneurons in the PMG of the microgyrus. These alterations may enhance inhibitory output of FS interneurons and serve to partially compensate for the increased excitatory drive onto pyramidal cells known to be present in the epileptogenic cortex (Jacobs and Prince 2004).

MATERIALS AND METHODS

Surgical procedures. All experiments were performed according to protocols approved by the Stanford Institutional Animal Care and Use Committee. In this study, we used litters of transgenic mice that specifically expressed GFP in cortical FS cells (mouse strain G42; Chattopadhyaya et al. 2004). Focal FLs were induced at postnatal day (P)0-P1 (P0 = date of birth) using a previously described method (Jacobs et al. 1996, 1999). Briefly, newborn mice were anaesthetized by immersing in ice until no responses were observed to tail pinch. The scalp was incised in the midline and retracted to expose the skull over the left hemisphere. A copper probe (1 × 3 mm rectangular shape) cooled with dry ice was placed for 5~7 s on the skull above the parietal cortex, 2~4 mm lateral and parallel to the midline. The scalp incision was then closed with Nexaband liquid tissue adhesive (Abbott Laboratories, North Chicago, IL). The pups were allowed to recover and were returned to the nurturing dam.

Slice preparation and electrophysiology. Brain slices were prepared and maintained using standard techniques (Jin et al. 2006). Mice at the age of P15–32 were deeply anesthetized with pentobarbital (55 mg/kg ip) and decapitated. The brain was rapidly removed and placed in ice cold (4°C) oxygenated slicing solution containing the following (in mM): 230 sucrose, 2.5 KCl, 1.25 NaH_2PO_4, 10 $MgSO_4{\cdot}7HO_2$, 10 glucose, 0.5 $CaCl_2{\cdot}2H_2O$, and 26 $NaHCO_3$. Coronal slices (350 μm) were cut with a vibratome (Lancer Series 1000; Vibratome, St. Louis, MO) through the lesioned sensorimotor cortex or the homotopic region of the naïve mice and maintained using standard techniques. After an ~0.5-h incubation at 32°C in standard artificial cerebral spinal fluid (ACSF), slices were kept at room temperature. The ACSF contained the following (in mM): 126 NaCl, 2.5 KCl, 1.25 NaH_2PO_4, 2 $CaCl_2$, 2 $MgSO_4{\cdot}7H_2O$, 26 $NaHCO_3$, and 10 glucose, pH 7.4 when saturated with 95% O_2-5% CO_2.

Patch electrodes were pulled from borosilicate glass tubing (1.5 mm OD) and had an impedance of 4–6 MΩ when filled with solution for voltage-clamp experiments containing the following (in mM): 120 Cs-gluconate, 10 KCl, 11 EGTA, 1 $CaCl_2{\cdot}{\cdot}2H_2O$, 2 $MgCl_2{\cdot}6H_2O$, 10 HEPES, 2 Na_2ATP, 0.5 NaGTP, and 0.5% biocytin. In current-clamp experiments, we used a K-gluconate-based intracellular solution containing the following (in mM): 95 K-gluconate, 40 KCl, 5 EGTA, 0.2 $CaCl_2{\cdot}2H_2O$, 10 HEPES, and 0.5% biocytin. The osmolarity of the pipette solutions was adjusted to 285–295 mosM and pH to 7.3 with 1 M KOH. Single slices were transferred to a recording chamber where they were minimally submerged in ACSF. Fifty micromoles of 2-amino-5-phosphonovaleric acid (APV) were added to prevent polysynaptic recurrent excitation and eliminate slow NMDA receptor activation.

The microsulcus in slices from lesioned animals was visualized readily under a microscope. Patch-clamp recordings were made from GFP-expressing FS cells in the PMG zone of the lesioned sensorimotor cortex or the homotopic region of the control slices, using infrared video microscopy (Zeiss Axioskop; Carl Zeiss) and a ×63 water-immersion lens (Achroplan ×63 0.9W; Carl Zeiss) and an Axopatch 200A amplifier (Axon Instruments, Foster City, CA). Access resistance was measured in voltage-clamp mode from responses to 5-mV depolarizing voltage pulses. Recordings with access resistance <25 MΩ and without significant (<25%) changes during the recording were used for data analysis. Membrane potentials were not corrected for liquid junction potentials. The responses were low-pass filtered at 2 kHz and recorded for later analysis. Excitatory postsynaptic currents (EPSCs) were measured at a holding potential of −70 mV. Inhibitory postsynaptic currents (IPSCs) were measured at +20 mV. Recording of IPSCs at this holding potential revealed no outward currents or only small inward currents that were mediated by AMPA receptor activation (see Fig. 5, *A* and *C*), which allowed us to efficiently isolate $GABA_A$ receptor mediated outward currents.

Photolysis of caged glutamate and stimulus patterns. In each experiment, we first recorded spontaneous (s)EPSCs and IPSCs for analysis of amplitude and frequency of synaptic events. Glutamate uncaging was then performed as described previously (Jin et al. 2006, 2011; Chu et al. 2010). Briefly, a frequency tripled Nd:YVO_4 laser (Series 3500 pulsed laser, ~1 W, 100-kHz repetition rate; DPSS Lasers, San Jose, CA) was interfaced with an upright microscope (Axioskop; Zeiss) through its epifluorescence port via a series of mirrors and lenses. Movement of the laser beam was controlled with mirror galvanometers (model 6210; Cambridge Technology, Cambridge, MA) that were triggered by scanning and data acquisition software developed by J. R. Huguenard. One-hundred micromoles of MNI-caged glutamate (4-methoxy-7-nitroindolinyl-caged L-glutamate; Tocris Bioscience) and 50 μM APV (Sigma) were added to 20 ml of recirculating regular ACSF at the beginning of each experiment. Focal photolysis of caged glutamate was accomplished by switching the UV laser to give a 400- to 800-μs light stimulus through a ×5 UV objective.

To separately evaluate the activation profile of cortical pyramidal and FS neurons, we mapped AP firing of these neurons in layers II-VI evoked by LSPS under current-clamp recording. Grids of photostimulation sites between 350 and 400 × 350 and 400 μm with 50-μm spacing were drawn around the recorded neurons. Durations of laser flashes were adjusted so that at least one AP could be recorded from each mapping area. This laser duration was determined at the beginning of a recording experiment and used for mapping synaptic connectivity. To map synaptic connectivity, a grid of 500~550 × 1,000~1,200 μm with 50-μm spacing between adjacent rows and columns was drawn to cover cortical layers II-VI. To avoid the effects of repetitive stimulation at any given spot, a pseudorandom stimulus sequence pattern with a 1-s interstimulus interval was used. In the majority of the mapped neurons, two to three maps were collected from each neuron and averaged to reduce the interference of spontaneous events.

Following the electrophysiological recordings, slices containing biocytin-filled neurons were fixed and processed with the standard avidin-biotin-peroxidase method or immunofluorescent staining (Jin et al. 2006). Labeled neurons were examined under light and confocal microscopy to verify their morphology and location.

Data acquisition and analysis. Neuronal intrinsic properties and AP firing were determined from responses to a series of 500-ms hyperpolarizing and depolarizing currents pulses (25- to 50-pA steps) under current-clamp mode. Resting membrane potential was measured as the membrane voltage when no current was injected. Input resistance was determined from the slope of a best-fit-line through the linear segment of a voltage-current relation. Membrane time constant was calculated by single-exponential fitting to the voltage response to hyperpolarizing current steps. The first AP elicited by lowest current injection was used for measuring AP properties. The AP threshold was determined at the level when voltage deflection exceeded 10

mV/ms. The duration of the AP was measured at its half maximal amplitude. AP amplitude was measured as the difference between AP threshold and the peak amplitude. AP afterhyperpolarization was measured as the difference between AP threshold and the most negative deflection after the AP.

Both spontaneous and evoked synaptic events were detected using an event detecting software (Jin et al. 2006). For each recording trace corresponding to an uncaging spot, we analyzed a 100-ms preuncaging period and a 50-ms uncaging window (see Fig. 3*A*). Because direct activation of non-NMDA glutamatergic receptors peaked within the first ~6 ms after laser flashes, events occurring during this time window were excluded from data analysis (see Fig. 3*A*, grey area). All EPSCs that occurred in a time window between 6 and 50 ms after photostimulation were regarded as uncaging evoked responses and summed to make a composite amplitude (see Fig. 3*A*, yellow area, *events a–e*). Evoked events that occurred and superimposed on a direct activation (i.e., *events a* and *b* in Fig. 3*A*) were measured after subtracting the amplitudes of the underlying direct activation. All IPSCs that occurred within 6–50 ms after laser flashes were included as evoked responses. Synaptic events were detected and analyzed using PSC detection software. To correct for contamination of spontaneous synaptic events (Kumar et al. 2007), we adjusted the composite PSC amplitude of each trace by subtracting an average PSC amplitude that was calculated by dividing the sum of all prestimulus spontaneous synaptic events in 100 ms in a map by the total trace number of the map and adjusted to an equal time period.

As in our previous studies, we used several parameters to quantify characteristics of synaptic connectivity (Deleuze and Huguenard 2006; Jin et al. 2006). "Hotspots" were sites on the stimulation grid from which at least one postsynaptic current was detected within the measurement window. "Hotspot ratio" was computed by dividing the number of hotspots in a row by the total number of uncaging spots in the row. "Hotspot amplitude" was computed by dividing the sum of peak amplitude of all detected events in a row by the number of hotspots in the row. "Composite amplitude" was defined as the sum of peak amplitudes of all detected synaptic events during the measurement window. Furthermore, to evaluate the strength and distribution of PSCs, a ''region normalized" EPSC or IPSC was obtained by dividing the sum of all composite amplitudes within a given row of stimulus sites along the horizontal axis by the total number of stimulus sites.

For spontaneous (s)EPSCs and IPSCs, cumulative probability of the intervals of sEPSCs and sIPSCs were generated by compiling 100 consecutive events from each neuron of the control and FL groups. Mean event frequencies and amplitudes were calculated and compared between the two groups.

Data are presented as means ± SE. Statistical analyses between the two groups in the hotspot ratio and hotspot amplitude were made with two-way ANOVA followed by Tukey post hoc test. Comparisons of cumulative probability plots between the control and FL groups were made using the Kolmogorov-Smirnov test. Statistical significance for group means was determined with a two-tailed Student's *t*-test with a $P < 0.05$. Origin and Microsoft Excel software were used to perform data analyses and statistical tests.

RESULTS

We used a line of transgenic mice expressing GFP in cortical FS cells (Chattopadhyaya et al. 2004). The FL was created at P0–1. As in previous experiments with FL rat pups (Jacobs et al. 1999), we did not observe obvious behavioral seizures during casual observations prior to the slice experiment. In coronal cortical slices prepared from FL mice at P15–32, the microgyrus was visible under microscope and commonly extended from the pia to layer V/VI or to the white matter (Fig. 1*B*, arrow). Because previous in vitro recordings in the FL model indicated that epileptiform activities occur in the PMG region (Jacobs et al. 1996, 1999; Luhmann et al. 1998), patch-clamp recordings were obtained from the PMG zone that was ~0.5–1.0 mm lateral to the edge of the microgyrus and from the homotopic region of the control cortex (Jacobs et al. 1996, 1999). In contrast to the microgyrus, the PMG zone maintained typical six-layered structure similar to normal cortex (Fig. 1*B*). Recordings for activation profile and synaptic activity were usually made from different slices of each mouse. Similar to our previous results (Jin et al. 2011), all GFP-expressing neurons exhibited fast nonadapting high-frequency AP firing and morphologies typical for basket cells with smooth multipolar dendrites and dense local axonal arbors in cortical layer V (Fig. 1, *C–F*). Passive membrane properties and AP properties of the FS cells were similar between the control and FL groups (Table 1).

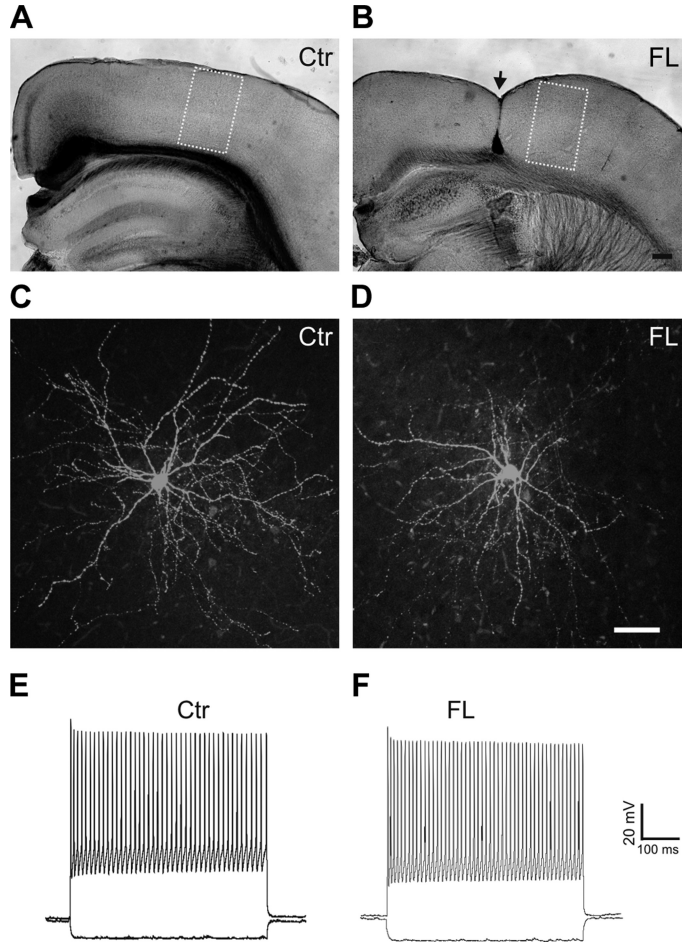

Fig. 1. Green fluorescent protein (GFP)-expressing fast spiking (FS) interneurons in the control (Ctr) and freeze lesion (FL) cortex. *A* and *B*: images of fixed coronal cortical sections from control (*A*) and FL (*B*) mice. The yellow rectangles delineate uncaging areas that cover ~500–600 × 1,000–1,200 μm of the cortex. The location of the FL lesion is marked with arrow in *B*. *C* and *D*: confocal images of biocytin-filled GFP-expressing neurons in layer V of control (*C*) and FL (*D*) neocortical slices processed with avidin D fluorescein reveal typical morphology of FS interneurons with smooth multipolar dendrites and dense local axonal arbors in cortical layer V. *E* and *F*: depolarizing current pulses in GFP neurons evoke high-frequency trains of fast action potentials without obvious adaptation in the control (*E*) and FL cortex (*F*). Scale bars = 200 μm in *B* for *A* and *B*; 50 μm in *D* for *C* and *D*.

Table 1. *Intrinsic properties of FS neurons*

Intrinsic Properties	Sham (n = 13)	FL (n = 12)
Resting membrane potential, mV	−59.1 ± 2.4	−59.4 ± 1.8
Input resistance, MΩ	90.6 ± 7.0	88.4 ± 9.5
Membrane time constant, ms	5.6 ± 0.7	7.0 ± 0.8
AP threshold, mV	−36.7 ± 2.0	−33.7 ± 2.0
AP amplitude, mV	59.9 ± 2.1	63.5 ± 1.3
AP duration, ms	0.40 ± 0.02	0.42 ± 0.02
AHP, mV	−12.6 ± 1.0	−10.7 ± 1.7

Values are means ± SE. FS, fast spiking; FL, freeze lesion; AP, action potential; AHP, afterhyperpolarization.

Similar activation profiles of neurons in the control and FL cortex. Changes in neuronal membrane responses to glutamate might differ between control and FL cortexes and affect AP firing and activation of synaptic events. Therefore, we first determined whether there were any differences in direct neuronal activation of APs induced by glutamate uncaging between pyramidal neurons and between FS cells of the control and FL cortex. In all AP maps, laser durations ranged between 300 and 800 μs, with means of 366 ± 19 and 379 ± 28 μs for the control and FL groups, respectively ($P > 0.05$, Student's t-test). Depolarizations and AP firing were evoked by uncaging stimuli that were mostly located near the recorded neuronal somata (Fig. 2, *A*, *B*, *G*, and *H*). In both pyramidal neurons and FS cells, the average maps of evoked APs were similar in size and intensity between the control and FL groups (Fig. 2, *A*, *B*, *G*, and *H*). For pyramidal neurons, 85 and 82% of the AP hotspots were located with 100 μm of somata in the control (n = 16) and FL (n = 9) groups, respectively. For the FS cells, 80 and 95% of the AP hotspots were located within 150 μm of somata in the control (n = 14) and FL (n = 15) groups, respectively. For both pyramidal neurons and FS cells, there were no significant differences between the control and FL groups in hotspot and spike number at different distances from the somata (Fig. 2, *C*, *D*, *I*, and *J*). For both pyramidal and FS neurons, there were also no significant differences in mean hotspot number per neuron, mean AP number per map, and mean AP per hotspot between the two groups (Fig. 2, *E* and *K*; Table 2). The results indicated that photostimulation of cortical neurons evoked similar and relatively focused direct activation in control and FL slices and that the observed differences in synaptic responses in FS interneurons between control and FL mice described below were attributable to differences in synaptic connectivity rather than differences in somatic responsiveness to glutamate uncaging.

Increased excitatory connectivity to layer V FS cells in the FL cortex. Previous studies showed enhancement in both excitatory and inhibitory synaptic connectivity to the layer V pyramidal neurons in the FL model in rats (Brill and Huguenard 2010). To further dissect the inhibitory circuits, we mapped monosynaptic excitatory connectivity onto layer V FS neurons in control and FL sensorimotor cortex. Whole cell voltage-clamp recordings were obtained from 25 control and 20 FL GFP-expressing FS neurons in layer V of the control and FL cortex (boxes in Fig. 1, *A* and *B*). Evoked EPSCs were separated from evoked direct dendritic and somatic depolarizations by excluding the responses that occurred within 6 ms following laser flashes (Fig. 3*A*). We constructed maps of excitatory synaptic input to individual FS neurons and compared input strength across cortical layers based on the composite EPSC amplitude evoked by uncaging at each spot and the fraction of hot spots at which EPSCs could be evoked (Jin et al. 2011). A sample map and recordings from an FS interneuron of the FL cortex are shown in Fig. 3, *B* and *C*. Average maps from all mapped FS neurons are shown in Fig. 3, *D* and *E*.

We analyzed the changes in the hotspot EPSC amplitude and hotspot ratio relative to the cortical depth of the uncaging stimulus. In the normal sensorimotor cortex, most excitatory input onto layer V FS neurons was from a region within 150–200 μm of the soma, within the extent of layer V; inputs from other layers contributed significantly less (Fig. 3*D*). In FS neurons of the FL group, the mean evoked EPSC amplitude at hotspots was not significantly different from that of the control group (Fig. 3, *F* and *H*; −24.7 ± 3.3 pA in control and −20.4 ± 1.1 pA in the FL groups; $P > 0.05$). In contrast, there was a small increase in the mean hotspot ratio in the FL vs. the control group that was significant in superficial layers of the cortex that spanned about 300–500 μm to cover about cortical layer IV (Fig. 3, *G* and *I*). When the hotspot ratios in all laminae were measured, they were 0.34 ± 0.02 in control and 0.37 ± 0.01 in FL group ($P < 0.05$). These data suggest that, compared with control cortex, layer V FS cells in the FL cortex received slightly more widespread excitatory synaptic input from intracortical neurons, without an increase in amplitude of individual hotspot responses.

Analysis of sEPSCs recorded in each neuron before the uncaging stimuli showed no significant differences in the amplitude or frequency for FS neurons in the PMG vs. control groups (Fig. 4, *A*–*D*). The mean sEPSC frequencies were 25.7 ± 3.2 Hz (n = 14) and 24.9 ± 2.9 Hz (n = 23) in the control and FL groups, respectively; the mean sEPSC amplitudes were −15.5 ± 0.6 and −14.4 ± 0.5 mV in the control and FL groups, respectively (Fig. 4, *C* and *D*; $P > 0.05$ in both comparisons).

Reduced inhibitory connectivity to layer V FS interneurons in the FL cortex. To determine whether there was any change in the inhibitory synaptic input to cortical FS cells in the PMG, we recorded sIPSCs and then mapped the inhibitory connectivity using LSPS and whole cell recordings with a Cs^+-based internal solution. There was no significant difference between the two groups in the amplitude of sIPSCs, with mean sIPSC amplitudes being 15.0 ± 0.7 and 16.0 ± 1.3 pA in the control and FL groups, respectively (Fig. 4*G*; $P > 0.05$). In contrast, the cumulative histogram of interevent intervals of the FL group was shifted to the right (Fig. 4*F*; $P < 0.05$, Kolmogorov-Smirnov test), indicating that the mean sIPSC frequency in the FL group was significantly lower than the control group. The mean sIPSC frequencies were 10.6 ± 1.4 Hz (n = 26) and 6.8 ± 0.9 Hz (n = 17) in the control and FL groups, respectively (Fig. 4*H*; $P < 0.05$).

Evoked IPSCs were recorded at holding potential of +20 mV. Uncaging stimuli evoked IPSCs as outward currents with a large variability in amplitude and latency. Amplitudes were as high as 400–500 pA at some hotspots, and the event latency ranged between ~3–10 ms from the laser flash (Fig. 5, *A* and *C*). In IPSC maps of both FL and control animals, events with large amplitude were evoked in a circular area of ~150 μm around somata in layer V (Fig. 5, *D* and *E*). Some events were also evoked from superficial or deep layers of the cortex. In

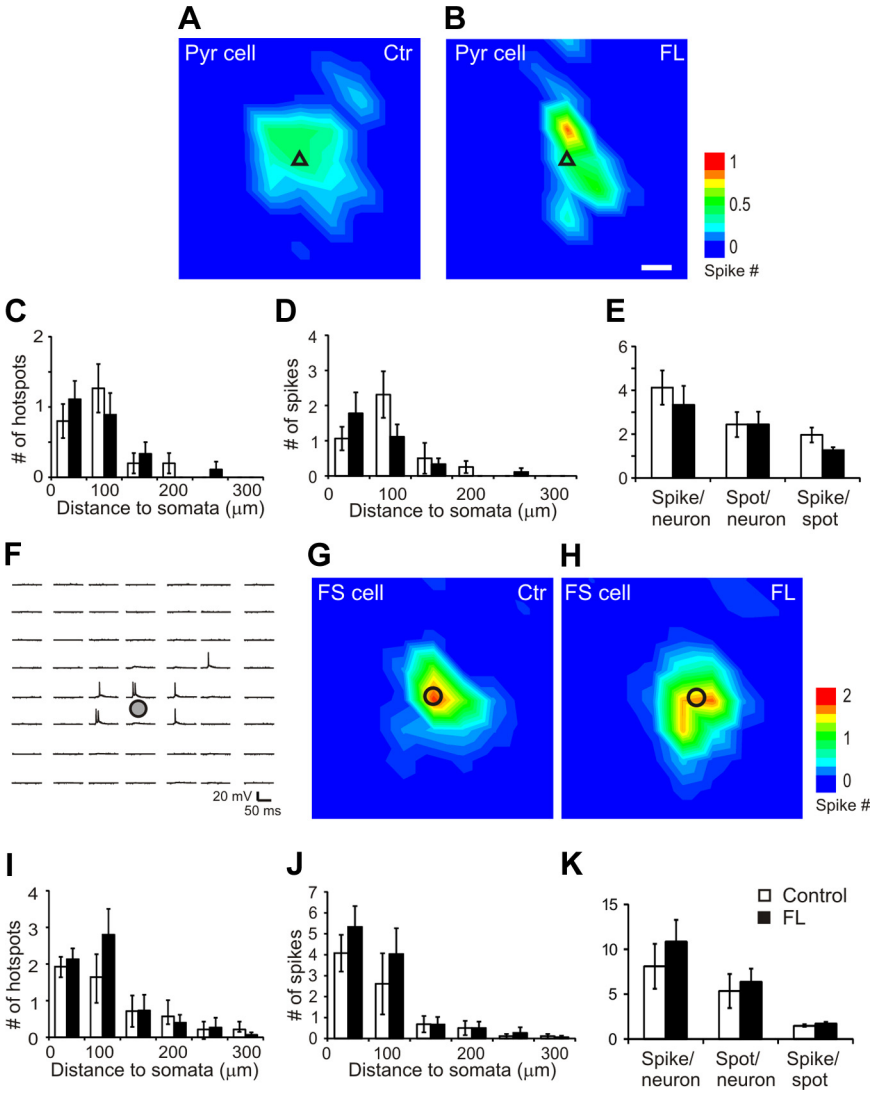

Fig. 2. Glutamate uncaging on neuronal somata induced similar direct excitation profiles of cortical pyramidal neurons and FS neurons in the control and FL neocortex. *A* and *B*: average action potential (AP) maps in pyramidal (Pyr) neurons in the control (*A*; $n = 16$) and FL cortex (*B*: $n = 9$). Most of the APs were activated by stimuli close to the somata of recorded neurons. Black triangles in *A* and *B* indicate somata of recorded pyramidal neurons. Scale bar in $B = 50$ μm for *A*, *B*, *G*, and *H*. *C–E*: analysis of maps in *A* and *B* showed that there were no significant differences between the control and FL groups in mean number of hotspots (*C*) and evoked APs (*D*) per map at different distances to somata. There were also no significant differences in the mean numbers of AP spikes per neuron, hotspot per neuron, and spikes per hotspot between the control and FL groups (*E*). *F*: representative map of uncaging evoked AP firing in a cortical layer V FS neuron. An area of 300 × 350 μm was photostimulated by UV laser flashes with a 50-μm spacing. Note that AP firing was triggered only in an area close to the soma. Black circles in *F–H* indicate somata of recorded FS cells. *G* and *H*: average AP maps in FS neurons in the control (*G*; $n = 14$) and FL cortex (*H*; $n = 15$). Most of the APs were activated by stimuli close to the somata of recorded neurons. Black circles indicate somata of recorded FS neurons. *I–K*: there were no significant differences between the control and FL groups in mean number of hotspots (*I*) and evoked APs (*J*) per map at different distances to FS neuron somata. There were also no significant differences in the average numbers of AP spikes per FS neuron, hotspot per FS neuron, and spikes per hotspot between the control and FL groups (*K*).

maps from FL mice, there was a significant reduction in the hotspot ratio compared with control maps (Fig. 5, *D–G*). The mean hotspot amplitudes were 21.6 ± 1.6 pA in the control and 18.2 ± 1.8 pA in the FL group ($P > 0.05$). The mean hotspot ratios were 0.37 ± 0.03 in the control and 0.29 ± 0.03 in the FL group ($P < 0.01$). The reductions in the hotspot ratio along the cortical depth were more significant in superficial (layer II-IV; $P < 0.05$) and deep (layer VI; $P < 0.05$) laminae than at the level of recorded somata in layer V (Fig. 5, *G* and *I*). These results suggest that contraction of inhibitory synaptic maps onto layer V FS cells was mainly caused by a reduction in the connectivity of functionally coupled presynaptic interneurons.

DISCUSSION

We used LSPS in combination with whole cell patch-clamp recordings to determine excitatory and inhibitory synaptic connectivity onto cortical layer V FS neurons in the FL model of cortical microgyria in mice. We mapped synaptic inputs onto these neurons in the PMG region of the FL cortex and found a significant increase in excitatory synaptic connectivity and a decrease in inhibitory synaptic connectivity onto them, similar, in some respects, to previously reported alterations in layer V pyramidal cells and FS interneurons in the partial cortical isolation ("undercut") model of posttraumatic epileptogenesis (Jin et al. 2006, 2011). In the absence of other abnormalities in FS interneurons, this combination of changes

Table 2. *Uncaging evoked AP spikes in cortical pyramidal neurons and FS neurons*

Group	Pyramidal Neurons			FS Neurons		
	Hotspots/map	Spikes/map	Spikes/hotspot	Hotspots/map	Spikes/map	Spikes/hotspot
Control	2.4 ± 0.6	4.1 ± 0.8	2.0 ± 0.3	5.4 ± 1.9	8.1 ± 2.5	1.5 ± 0.2
FL	2.4 ± 0.6	3.3 ± 0.9	1.3 ± 0.1	6.4 ± 1.5	10.9 ± 2.5	1.7 ± 0.2

Values are means ± SE.

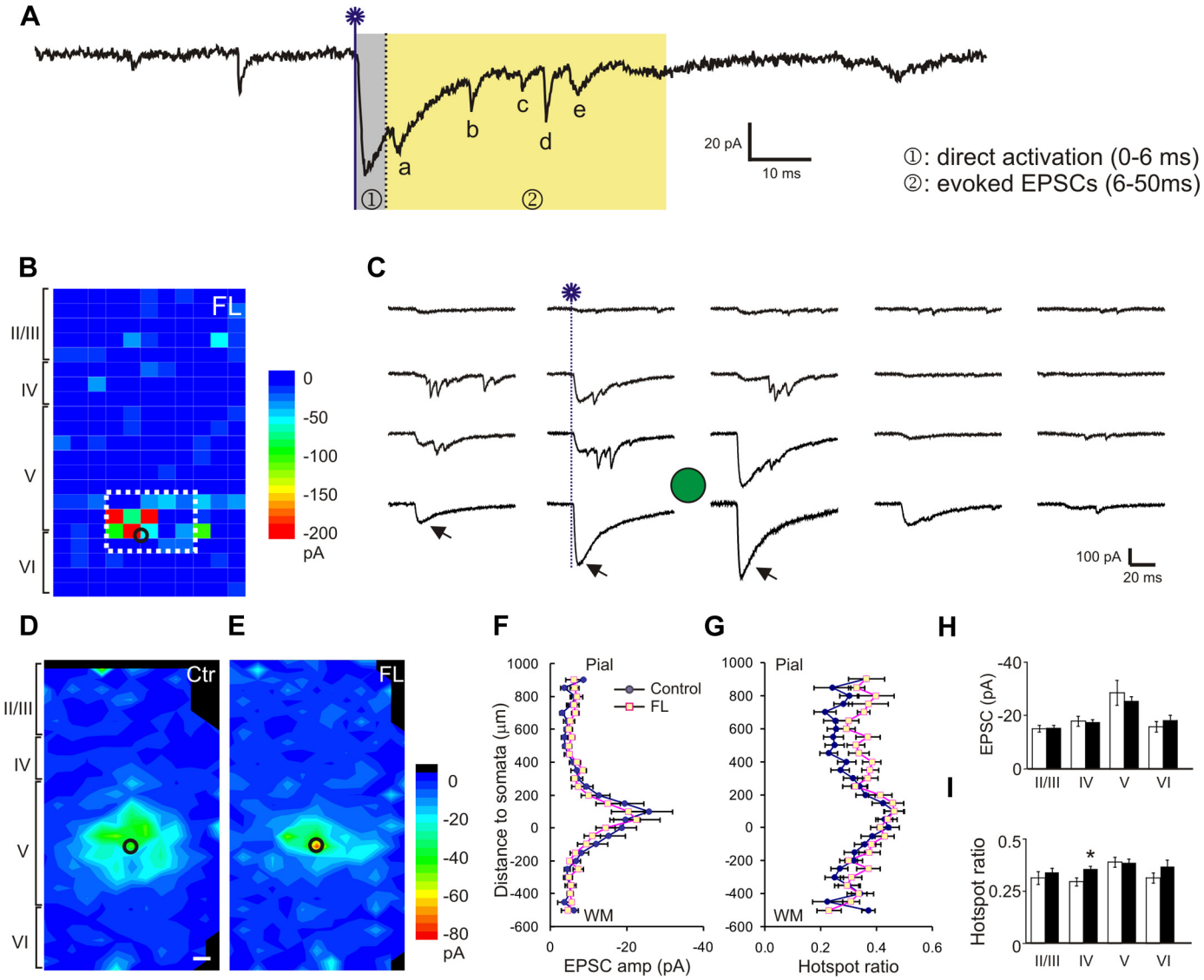

Fig. 3. Enhancement of excitatory synaptic input onto layer V FS interneurons in the FL cortex. *A*: trace from a representative recording showing measurement of uncaging evoked events. Glutamate uncaging (blue line with a star; same in the following figures) caused direct activation of neuronal soma, which usually peaked within 6 ms (gray area). Evoked excitatory postsynaptic currents (EPSCs) were detected in a time window between 6 and 50 ms after laser flashes (*events a–e* in the yellow area) and were summed to generate a composite EPSC. *B*: representative uncaging map of a FS neuron in the FL cortex. The composite amplitude for each spot was color-coded and its location plotted relative to the slice. The distance between neighboring uncaging spots in *B* and *C* and Fig. 5, *B* and *C*, was 50 μm. *C*: 5 columns of traces show responses evoked by corresponding 5 columns of uncaging spots inside the white rectangle in *B*. The arrows indicate responses of direct activation. The black or green circles in *B–E* and Fig. 5, *B–E*, mark the location of FS neurons. *D* and *E*: average maps of the composite amplitude of EPSCs in layer V FS cells of the control (*C*; $n = 25$) and FL (*D*; $n = 20$) groups. The color scale bar indicates mean composite EPSC amplitude; black areas indicate no mean values available. The scale bars in Fig. 3*D* and Fig. 5*D*: 50 μm. *F* and *G*: mean hotspot EPSC amplitude (*E*) and mean hotspot ratio (*F*) at various vertical distances from somata in the control and FL groups. There was a significant increase in hotspot ratio in the FL group ($P < 0.05$, two-way ANOVA). *y*-Axis scale: 0 = position of somata in layer V; positive numbers: toward pial surface; negative toward white matter. *H*: mean hotspot amplitudes from different cortical layers to layer V FS cells were similar between the FL and control groups. *I*: mean hotspot ratio in layer IV area was higher in the FL group than the control (*$P < 0.05$), but there were no significant differences in other cortical layers.

in synaptic weights might be expected to result in a net increase in excitation of layer V FS neurons and strengthen their inhibitory output. Previous results have shown increased inhibitory synaptic efficacy in this model (Jacobs and Prince 2004; Brill and Huguenard 2010), and the current data provide further information on the changes in the inhibitory network.

FLs in the mouse neocortex generate four-layer cortical microgyri, similar to those observed in rats (Fig. 1; Shimizu-Okabe et al. 2007; Wang et al. 2014). The mice used for this experiment were between P15 and 32, an age range after major developmental changes in electrophysiological properties of the FS neurons (see refs below). Compared with FS cells at younger ages, these neurons exhibit typical intrinsic properties of FS interneurons, such as lower input resistance, fast membrane time constant, brief AP duration, and high AP firing rate (Pangratz-Fuehrer and Hestrin 2011; Yang et al. 2012). Studies using paired patch-clamp recordings have shown that the probabilities of synaptic coupling between FS cells and between FS and pyramidal neurons increase dramatically after P11–12 and remain relatively stable at this level up to the observed age of P30 (Pangratz-Fuehrer and Hestrin 2011; Yang et al. 2012). However, it is likely that some developmen-

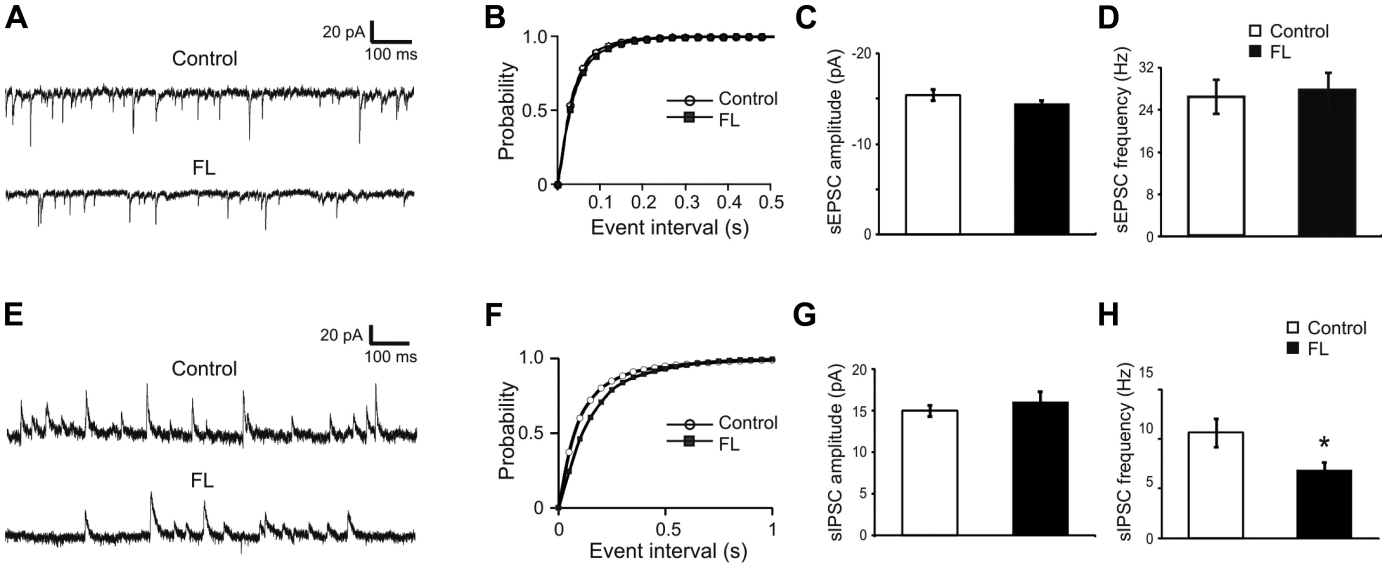

Fig. 4. No significant changes in the frequency and amplitude of spontaneous (s)EPSCs in FS cells of the FL neocortex but reduced frequency of sIPSCs in these cells. *A*: representative traces of sEPSCs recorded from FS cells of the control (*top*) and FL (*bottom*) neocortex. *B*: cumulative histogram of sEPSC intervals. There was no significant difference between the 2 groups ($P > 0.05$, Kolmogorov-Smirnov test). *C* and *D*: mean amplitudes and frequencies of sEPSC were similar between the control and FL groups. *E*: representative traces of sIPSCs recorded from FS cells of the control (*top*) and FL (*bottom*) neocortex. *F*: cumulative plot of sIPSC intervals. There was a significant difference between the 2 groups ($P < 0.01$, Kolmogorov-Smirnov test). *G* and *H*: mean amplitudes of sIPSC in FS cells were similar between the control and FL groups, but the sIPSC frequency in the FL group was significantly lower than the control group. *$P < 0.05$.

tal changes are still occurring at this stage, and we cannot rule out the possibility that the FL injury, by affecting these developmental processes, contributes to the shifts in synaptic innervation of interneurons reported here. Also, results might differ at longer latencies between the FL and mapping experiment (Jacobs et al 1999; Rosen et al 1998).

We found a small but significant increase in the hotspot ratio for laser-evoked EPSCs in layer V FS interneurons of the FL cortex. These interneurons normally receive the majority of their excitatory synaptic input from layer V and less from superficial cortical layers (Fig. 3) (Thomson and Bannister 2003). The increase in the hotspot ratio of the EPSC maps could be attributed to a higher density of presynaptic excitatory neurons in these layers of the PMG region of the FL cortex so that uncaging at a given spot would activate more presynaptic cells. However, this possibility is not supported by results from earlier studies showing no change in the density of cortical neurons in the PMG region of the FL cortex in rats (Jacobs et al. 1996). A more reasonable explanation may be that axon sprouting or failure in axon pruning of excitatory neurons during development results in enhanced synaptic connectivity onto the FS neurons in layer V. Axon sprouting is a common pathological change after various brain insults that may underlie neocortical and temporal lobe epileptogenesis (Sutula et al. 1989, 1995; Salin et al. 1995; Buckmaster et al. 2002). Failure in axonal pruning and synapse elimination may also result in increased axonal arbors and/or increased density of synapses, leading to epileptogenesis in the cortex or hippocampus (Galvan et al. 2000; Chu et al. 2010). Enhanced axonal innervation from pyramidal neurons to FS cells would also result in an increase in the frequency of sEPSCs. However, we observed no significant changes in sEPSC frequency and amplitude in the FL cortex. Because mapping with LSPS mostly reveals action potential-dependent synaptic release while recording sEPSCs mainly detects action potential-independent release (Li and Prince 2001), a difference between these two methods may contribute to this discrepancy. However, a more straightforward explanation may be the small yet statistically significant difference in the hotspot ratio between the two groups (0.35 in the control vs. 0.37 in the FL groups). This layer-specific difference in the hotspot ratio (Fig. 3*G*) may easily become undetectable in sEPSCs recording, in which events from all sources are pooled together. Indeed, significant difference in the mean hotspot ratio was detected only in cortical layer IV. Previous studies in the FL microgyrus model in rats found increases in both spontaneous and miniature EPSCs (sEPSCs and mEPSCs) and an expansion of excitatory input maps in layer V pyramidal neurons (Jacobs and Prince 2004; Brill and Huguenard 2010). Similarly, results of a study in the irradiated model of cortical dysplasia in rats indicated an increase in the density of excitatory synapses (Zhou and Roper 2010). These changes are consistent with axon sprouting, which results in an increased number of excitatory neurons innervating layer V pyramidal neurons. Sprouting axons can make synapses not only on excitatory neurons, but also on interneurons, particularly parvalbumin-containing neurons (Kotti et al. 1997; Sloviter et al. 2006). Although it is unclear whether there is an increase in the length of axonal arbors or bouton density in the FL cortex, the increase in the fraction of sites from which EPSCs are evoked strongly suggests axon sprouting and formation of new synapses. These changes may contribute to the spatially more extensive functional excitatory connections from cortical pyramidal neurons onto layer V FS neurons. LSPS stimulation did not evoke EPSCs of larger amplitude in the layer V interneurons in PMG cortex. This suggests that, as in other models of injury-induced sprouting (e.g., McKinney et al. 1997), the strength of excitatory contacts onto individual cells (interneurons in this case) may not be increased, even though the network connectivity is expanded.

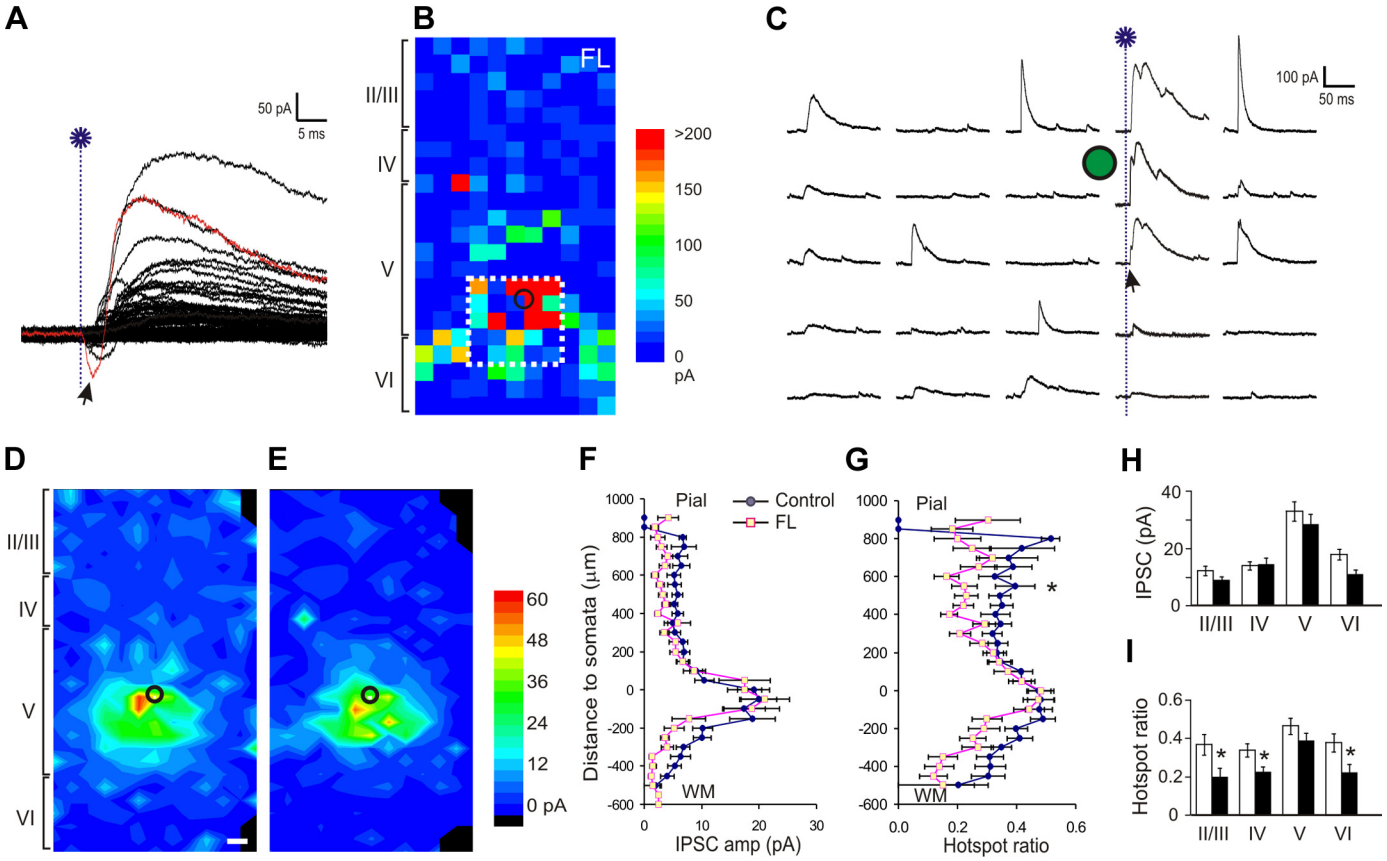

Fig. 5. Reduction in inhibitory synaptic input onto layer V FS interneurons in the FL cortex. *A*: representative traces of uncaging evoked IPSCs in a map that were recorded at +20 mV. At this holding potential, uncaging-evoked directly activated AMPA receptor currents were small and inward (arrow) or invisible (arrow in *C*), and the IPSCs were outward, large, and readily differentiated from EPSCs. *B*: representative uncaging-evoked IPSC map of the FL cortex. For each uncaging spot, evoked IPSCs were detected in a time window between 0 and 50 ms after laser flashes and summed. The resulting composite amplitude for each spot was plotted and color coded as in Fig. 3. *C*: traces show the responses of uncaging spots inside the white rectangle in *B*. The onset of laser flash in the 4th column is marked with a blue dotted line. Note the large variability in the amplitude and waveform among different traces. *D* and *E*: average maps of the composite amplitude of IPSCs in layer V FS cells of the control (*D*; $n = 26$) and FL (*E*; $n = 18$) groups. Responses were evoked from more widespread cortical areas in control group. Black circles: cell location. *F* and *G*: mean hotspot IPSC amplitudes (*E*) and mean hotspot ratio (*F*) at various vertical distances from somata in the control and FL groups. There was no significant difference in hotspot amplitude (*F*), but there was a significant difference in hotspot ratio between the 2 groups ($P > 0.05$ in hotspot amplitude and $P < 0.05$ in hotspot ratio). A significant decrease in hotspot ratio was present between 500 and 550 μm superficial to the neuronal somata. The *y*-axis is labeled as in Fig. 3, *E* and *F*. *H*: there were no significant differences between the 2 groups in hotspot amplitudes of the evoked IPSCs. *I*: when the data were grouped according to cortical layers, hotspot ratios were significantly lower in layers II/III, IV, and VI of the FL group than the control group. $*P < 0.05$.

IPSCs evoked by glutamate uncaging varied greatly in amplitude and waveform. Consistent with previous mapping results of IPSCs from layer V pyramidal and FS neurons in microgyri of rats (Brill and Huguenard 2009), events with large amplitude and short latencies were often evoked in the vicinity of somata (Fig. 5, *B* and *C*). IPSCs from presynaptic FS neurons have faster rise times and larger amplitudes compared with those from non-FS neurons such as low threshold-spiking interneurons (Xiang et al. 2002; Bacci et al. 2003; Brill and Huguenard 2009; Otsuka and Kawaguchi 2009). We found both types of IPSCs in our LSPS maps of layer V FS neurons (Fig. 5*C*), suggesting that these neurons receive synaptic input from both FS and non-FS neurons. Although the vast majority of the evoked events were clearly monosynaptic, high-amplitude, polyphasic IPSCs were also observed in some neurons, particularly in regions close to the somata (Fig. 5*C*). It is not clear whether these PSCs are polysynaptic events or the spatial or temporal summation of monosynaptic IPSCs generated by both FS and non-FS interneurons. The convergence of these two different types of synaptic events onto single FS neurons may be responsible for the large amplitude and polyphasic waveforms in our IPSC maps, although the possibility of polysynaptic origin of these events cannot be completely excluded. We also found a reduction in IPSC maps of layer V FS cells in the FL cortex that is mainly due to a decrease in the hotspot ratios across different cortical layers, i.e., there were fewer sites from which uncaging could evoke IPSCs. This result suggests that fewer presynaptic interneurons or terminals effectively connected to the FS cells. We also observed a significant decrease in sIPSC frequency in the FS cells. These changes may result from structural alterations such as a reduced number of interneurons in the PMG (Rosen et al. 1998) or alterations in their total axonal length and a decreased number of GABAergic synapses such as occurs after cortical injury in mature rats (Prince et al. 2012) and other models of epileptogenesis (Ribak and Reiffenstein 1982; Defazio and Hablitz 1999; Kumar and Buckmaster 2006). In addition, decreased release probability from inhibitory terminals may contribute (Faria and Prince 2010; Ma and Prince 2012).

A normal density and distribution pattern of FS neurons is maintained in the PMG region of the rat FL cortex after P21, as revealed by immunostaining for parvalbumin in earlier studies (Jacobs et al. 1996; Hablitz and DeFazio 1998; Schwarz et al. 2000; but see Rosen et al. 1998). In contrast, somatostatin-expressing neurons decrease by 20% in areas adjacent to the FL at P30–32 in rats (Patrick et al. 2006). This decrease follows, rather than precedes, the onset of epileptiform activity (P12–18); however, it may contribute to the observed decrease in the hotspot ratio in our experiments. As somatostatin-expressing interneurons contribute to interlaminar inhibition through their broad axonal arbors (Dumitriu et al. 2007), a change in their density in the PMG may be responsible for the observed decrease in the hotspot ratio in the superficial and deep layers of the cortex. Because of different vulnerabilities and responses to the FL injury, different subtypes of cortical interneuron likely make different contributions to changes in inhibitory input to FS neurons (Kharazia et al. 2003).

An increase in excitatory connectivity and a decrease in GABAergic connectivity to the FS neurons may result in an increase in inhibitory synaptic output in the FL, which contrasts with results in other models of maldevelopment where there is a reduction in IPSC frequency (Zhu and Roper 2000; Chen and Roper 2003). Decreased inhibition is also reported in human focal cortical dysplasia (Calcagnotto et al. 2005). Reductions in IPSCs may result from decreases in interneuronal density (see references above), alterations in postsynaptic $GABA_A$ receptors (Zilles et al. 1998; Defazio and Hablitz 1999), decreased release of GABA at altered presynaptic terminals (Faria and Prince 2010; Faria et al. 2012; Ma and Prince 2012), and a variety of other mechanisms (reviewed in Li et al. 2011; Prince et al. 2012). Different structural types of malformation are associated with a variety of abnormalities including loss of subtypes of neurons, abnormal intrinsic neuronal properties, and altered patterns of migration, depending on the timing of the pathological process during stages of cortical development. It is therefore expected that the spectrum of mechanisms underlying associated neurological abnormalities, such as epileptogenesis and effects on postsynaptic inhibition, will differ significantly depending on the etiology and classification of a given malformation.

The principal results of these experiments are that layer V FS cells in the FL cortex receive more widespread excitatory synaptic inputs from intracortical neurons, without an increase in amplitude of individual hotspot responses and have reduced inhibitory synaptic connectivity from superficial and deep cortical layers. The dense local axonal arbors of the FS neurons mediate their inhibitory output onto both pyramidal cells and other interneurons in layer V (Kawaguchi and Kubota 1997). Thus the increased excitatory and reduced inhibitory drive to these FS interneurons might enhance their inhibitory output, which is consistent with enhanced synaptic inhibition observed in layer V pyramidal neurons of the PMG region of the FL cortex (Jacobs and Prince 2004; Brill and Huguenard 2010). Similarly, enhanced inhibition is also shown in hippocampal CA1 pyramidal cells of the *lis1* gene mutation model of lissencephaly (Jones and Baraban 2007). Because the expressions of potassium chloride cotrasporter-2 (KCC2) and sodium potassium chloride cotransporter-1 (NKCC1) are unaltered in neurons of the PMG region of the FL cortex (Shimizu-Okabe et al. 2007), it is likely that a low concentration of intracellular chloride is normally maintained and the efficacy of GABAergic inhibition is not impaired (e.g., Bonislawski et al. 2007; Jin et al. 2005). An enhancement in inhibitory synaptic output may not only play a role in maintaining a balance between excitation and inhibition in the malformed cortex but may also contribute to the synchronization of excitatory epileptiform activity (Michelson and Wong 1994; Khazipov and Holmes 2003).

ACKNOWLEDGMENTS

We thank Isabel Parada for valuable assistance with immunocytochemistry.

GRANTS

This work was supported by the National Institute of Neurological Disorders and Stroke Grants 5K99-NS-57940-2 (to X. Jin), NS-12151 (to D. Prince), and NS-39579 (to D. Prince) and National Institute of Drug Abuse Grant DA-15043.

DISCLOSURES

No conflicts of interest, financial or otherwise, are declared by the author(s).

AUTHOR CONTRIBUTIONS

Author contributions: X.J. and D.A.P. conception and design of research; X.J. performed experiments; X.J. and K.J. analyzed data; X.J., K.J., and D.A.P. interpreted results of experiments; X.J. and K.J. prepared figures; X.J. drafted manuscript; X.J. and D.A.P. approved final version of manuscript; D.A.P. edited and revised manuscript.

REFERENCES

Bacci A, Rudolph U, Huguenard JR, Prince DA. Major differences in inhibitory synaptic transmission onto two neocortical interneuron subclasses. *J Neurosci* 23: 9664–9674, 2003.

Barkovich AJ, Kjos BO. Nonlissencephalic cortical dysplasias: correlation of imaging findings with clinical deficits. *AJNR Am J Neuroradiol* 13: 95–103, 1992.

Barkovich AJ, Lindan CE. Congenital cytomegalovirus infection of the brain: imaging analysis and embryologic considerations. *AJNR Am J Neuroradiol* 15: 703–715, 1994.

Barkovich AJ, Rowley H, Bollen A. Correlation of prenatal events with the development of polymicrogyria. *AJNR Am J Neuroradiol* 16: 822–827, 1995.

Barth PG. Disorders of neuronal migration. *Can J Neurol Sci* 14: 1–16, 1987.

Bonislawski DP, Schwarzbach EP, Cohen AS. Brain injury impairs dentate gyrus inhibitory efficacy. *Neurobiol Dis* 25: 163–169, 2007.

Brill J, Huguenard JR. Enhanced infragranular and supragranular synaptic input onto layer 5 pyramidal neurons in a rat model of cortical dysplasia. *Cereb Cortex* 20: 2926–2938, 2010.

Brill J, Huguenard JR. Robust short-latency perisomatic inhibition onto neocortical pyramidal cells detected by laser-scanning photostimulation. *J Neurosci* 29: 7413–7423, 2009.

Buckmaster PS, Zhang GF, Yamawaki R. Axon sprouting in a model of temporal lobe epilepsy creates a predominantly excitatory feedback circuit. *J Neurosci* 22: 6650–6658, 2002.

Calcagnotto ME, Paredes MF, Tihan T, Barbaro NM, Baraban SC. Dysfunction of synaptic inhibition in epilepsy associated with focal cortical dysplasia. *J Neurosci* 25: 9649–9657, 2005.

Chattopadhyaya B, Di Cristo G, Higashiyama H, Knott GW, Kuhlman SJ, Welker E, Huang ZJ. Experience and activity-dependent maturation of perisomatic GABAergic innervation in primary visual cortex during a postnatal critical period. *J Neurosci* 24: 9598–9611, 2004.

Chen HX, Roper SN. Reduction of spontaneous inhibitory synaptic activity in experimental heterotopic gray matter. *J Neurophysiol* 89: 150–158, 2003.

Chu Y, Jin X, Parada I, Pesic A, Stevens B, Barres B, Prince DA. Enhanced synaptic connectivity and epilepsy in C1q knockout mice. *Proc Natl Acad Sci USA* 107: 7975–7980, 2010.

Defazio RA, Hablitz JJ. Reduction of zolpidem sensitivity in a freeze lesion model of neocortical dysgenesis. *J Neurophysiol* 81: 404–407, 1999.

DeFelipe J. Types of neurons, synaptic connections and chemical characteristics of cells immunoreactive for calbindin-D28K, parvalbumin and calretinin in the neocortex. *J Chem Neuroanat* 14: 1–19, 1997.

Deleuze C, Huguenard JR. Distinct electrical and chemical connectivity maps in the thalamic reticular nucleus: potential roles in synchronization and sensation. *J Neurosci* 26: 8633–8645, 2006.

Dulla CG, Tani H, Brill J, Reimer RJ, Huguenard JR. Glutamate biosensor imaging reveals dysregulation of glutamatergic pathways in a model of developmental cortical malformation. *Neurobiol Dis* 49C: 232–246, 2012.

Dumitriu D, Cossart R, Huang J, Yuste R. Correlation between axonal morphologies and synaptic input kinetics of interneurons from mouse visual cortex. *Cereb Cortex* 17: 81–91, 2007.

Dvorak K, Feit J. Migration of neuroblasts through partial necrosis of the cerebral cortex in newborn rats-contribution to the problems of morphological development and developmental period of cerebral microgyria. *Acta Neuropathol* 38: 203–212, 1977.

Faria LC, Parada I, Prince DA. Interneuronal calcium channel abnormalities in posttraumatic epileptogenic neocortex. *Neurobiol Dis* 45: 821–828, 2012.

Faria LC, Prince DA. Presynaptic inhibitory terminals are functionally abnormal in a rat model of posttraumatic epilepsy. *J Neurophysiol* 104: 280–290, 2010.

Freund TF, Katona I. Perisomatic inhibition. *Neuron* 56: 33–42, 2007.

Galvan CD, Hrachovy RA, Smith KL, Swann JW. Blockade of neuronal activity during hippocampal development produces a chronic focal epilepsy in the rat. *J Neurosci* 20: 2904–2916, 2000.

Gropman AL, Barkovich AJ, Vezina LG, Conry JA, Dubovsky EC, Packer RJ. Pediatric congenital bilateral perisylvian syndrome: clinical and MRI features in 12 patients. *Neuropediatrics* 28: 198–203, 1997.

Guerrini R, Andermann E, Avoli M, Dobyns WB. Cortical dysplasias, genetics, epileptogenesis. *Adv Neurol* 79: 95–121, 1999.

Guerrini R, Filippi T. Neuronal migration disorders, genetics, and epileptogenesis. *J Child Neurol* 20: 287–299, 2005.

Hablitz JJ, DeFazio T. Excitability changes in freeze-induced neocortical microgyria. *Epilepsy Res* 32: 75–82, 1998.

Jacobs KM, Gutnick MJ, Prince DA. Hyperexcitability in a model of cortical maldevelopment. *Cereb Cortex* 6: 514–523, 1996.

Jacobs KM, Hwang BJ, Prince DA. Focal epileptogenesis in a rat model of polymicrogyria. *J Neurophysiol* 81: 159–173, 1999.

Jacobs KM, Prince DA. Excitatory and inhibitory postsynaptic currents in a rat model of epileptogenic microgyria. *J Neurophysiol* 93: 687–696, 2004.

Jin X, Huguenard JR, Prince DA. Impaired Cl^- extrusion in layer V pyramidal neurons of chronically injured epileptogenic neocortex. *J Neurophysiol* 93: 2117–2126, 2005.

Jin X, Huguenard JR, Prince DA. Reorganization of inhibitory synaptic circuits in rodent chronically injured epileptogenic neocortex. *Cereb Cortex* 21: 1094–1104, 2011.

Jin X, Prince DA, Huguenard JR. Enhanced excitatory synaptic connectivity in layer v pyramidal neurons of chronically injured epileptogenic neocortex in rats. *J Neurosci* 26: 4891–4900, 2006.

Jones DL, Baraban SC. Characterization of inhibitory circuits in the malformed hippocampus of Lis1 mutant mice. *J Neurophysiol* 98: 2737–2746, 2007.

Kawaguchi Y, Kubota Y. GABAergic cell subtypes and their synaptic connections in rat frontal cortex. *Cereb Cortex* 7: 476–486, 1997.

Kellinghaus C, Moddel G, Shigeto H, Ying Z, Jacobsson B, Gonzalez-Martinez J, Burrier C, Janigro D, Najm IM. Dissociation between in vitro and in vivo epileptogenicity in a rat model of cortical dysplasia. *Epileptic Disord* 9: 11–19, 2007.

Kharazia VN, Jacobs KM, Prince DA. Light microscopic study of GluR1 and calbindin expression in interneurons of neocortical microgyral malformations. *Neuroscience* 120: 207–218, 2003.

Khazipov R, Holmes GL. Synchronization of kainate-induced epileptic activity via GABAergic inhibition in the superfused rat hippocampus in vivo. *J Neurosci* 23: 5337–5341, 2003.

Kotti T, Riekkinen PJ Sr, Miettinen R. Characterization of target cells for aberrant mossy fiber collaterals in the dentate gyrus of epileptic rat. *Exp Neurol* 146: 323–330, 1997.

Kumar SS, Buckmaster PS. Hyperexcitability, interneurons, and loss of GABAergic synapses in entorhinal cortex in a model of temporal lobe epilepsy. *J Neurosci* 26: 4613–4623, 2006.

Kumar SS, Jin X, Buckmaster PS, Huguenard JR. Recurrent circuits in layer II of medial entorhinal cortex in a model of temporal lobe epilepsy. *J Neurosci* 27: 1239–1246, 2007.

Li H, McDonald W, Parada I, Faria L, Graber K, Takahashi DK, Ma Y, Prince D. Targets for preventing epilepsy following cortical injury. *Neurosci Lett* 497: 172–176, 2011.

Li H, Prince DA. Synaptic activity in chronically injured epileptogenic sensory-motor neocortex. *J Neurophysiol* 88: 2–12, 2001.

Luhmann HJ, Raabe K, Qu M, Zilles K. Characterization of neuronal migration disorders in neocortical structures: extracellular in vitro recordings. *Eur J Neurosci* 10: 3085–3094, 1998.

Ma Y, Prince DA. Functional alterations in GABAergic fast-spiking interneurons in chronically injured epileptogenic neocortex. *Neurobiol Dis* 47: 102–113, 2012.

McBride MC, Kemper TL. Pathogenesis of four-layered microgyric cortex in man. *Acta Neuropathol* 57: 93–98, 1982.

McKinney RA, Debanne D, Gahwiler BH, Thompson SM. Lesion-induced axonal sprouting and hyperexcitability in the hippocampus in vitro: implications for the genesis of posttraumatic epilepsy. *Nat Med* 3: 990–996, 1997.

Michelson HB, Wong RK. Synchronization of inhibitory neurones in the guinea-pig hippocampus in vitro. *J Physiol* 477: 35–45, 1994.

Montenegro MA, Guerreiro MM, Lopes-Cendes I, Guerreiro CA, Cendes F. Interrelationship of genetics and prenatal injury in the genesis of malformations of cortical development. *Arch Neurol* 59: 1147–1153, 2002.

Otsuka T, Kawaguchi Y. Cortical inhibitory cell types differentially form intralaminar and interlaminar subnetworks with excitatory neurons. *J Neurosci* 29: 10533–10540, 2009.

Palmini A, Najm I, Avanzini G, Babb T, Guerrini R, Foldvary-Schaefer N, Jackson G, Luders HO, Prayson R, Spreafico R, Vinters HV. Terminology and classification of the cortical dysplasias. *Neurology* 62: S2–8, 2004.

Pangratz-Fuehrer S, Hestrin S. Synaptogenesis of electrical and GABAergic synapses of fast-spiking inhibitory neurons in the neocortex. *J Neurosci* 31: 10767–10775, 2011.

Patrick SL, Connors BW, Landisman CE. Developmental changes in somatostatin-positive interneurons in a freeze-lesion model of epilepsy. *Epilepsy Res* 70: 161–171, 2006.

Peters O, Redecker C, Hagemann G, Bruehl C, Luhmann HJ, Witte OW. Impaired synaptic plasticity in the surround of perinatally acquired [correction of aquired] dysplasia in rat cerebral cortex. *Cereb Cortex* 14: 1081–1087, 2004.

Piao X, Hill RS, Bodell A, Chang BS, Basel-Vanagaite L, Straussberg R, Dobyns WB, Qasrawi B, Winter RM, Innes AM, Voit T, Ross ME, Michaud JL, Descarie JC, Barkovich AJ, Walsh CA. G protein-coupled receptor-dependent development of human frontal cortex. *Science* 303: 2033–2036, 2004.

Prince DA, Jacobs KM, Salin PA, Hoffman S, Parada I. Chronic focal neocortical epileptogenesis: does disinhibition play a role? *Can J Physiol Pharmacol* 75: 500–507, 1997.

Prince DA, Parada I, Graber K. Traumatic brain injury and posttraumatic epilepsy. In: *Jasper's Basic Mechanisms of the Epilepsies*, edited by Noebels JL, Avoli M, Rogawski MA, Olsen RW, Delgado-Escueta AV. Bethesda, MD: National Center for Biotechnology Information, 2012.

Redecker C, Hagemann G, Kohling R, Straub H, Witte OW, Speckmann EJ. Optical imaging of epileptiform activity in experimentally induced cortical malformations. *Exp Neurol* 192: 288–298, 2005.

Redecker C, Luhmann HJ, Hagemann G, Fritschy JM, Witte OW. Differential downregulation of GABAA receptor subunits in widespread brain regions in the freeze-lesion model of focal cortical malformations. *J Neurosci* 20: 5045–5053, 2000.

Ribak CE, Reiffenstein RJ. Selective inhibitory synapse loss in chronic cortical slabs: a morphological basis for epileptic susceptibility. *Can J Physiol Pharmacol* 60: 864–870, 1982.

Roper SN, Yachnis AT. Cortical dysgenesis and epilepsy. *Neuroscientist* 8: 356–371, 2002.

Rosen GD, Jacobs KM, Prince DA. Effects of neonatal freeze lesions on expression of parvalbumin in rat neocortex. *Cereb Cortex* 8: 753–761, 1998.

Salin P, Tseng GF, Hoffman S, Parada I, Prince DA. Axonal sprouting in layer V pyramidal neurons of chronically injured cerebral cortex. *J Neurosci* 15: 8234–8245, 1995.

Scantlebury MH, Ouellet PL, Psarropoulou C, Carmant L. Freeze lesion-induced focal cortical dysplasia predisposes to atypical hyperthermic seizures in the immature rat. *Epilepsia* 45: 592–600, 2004.

Schwarz P, Stichel CC, Luhmann HJ. Characterization of neuronal migration disorders in neocortical structures: loss or preservation of inhibitory interneurons? *Epilepsia* 41: 781–787, 2000.

Shimizu-Okabe C, Okabe A, Kilb W, Sato K, Luhmann HJ, Fukuda A. Changes in the expression of cation-Cl^- cotransporters, NKCC1 and KCC2, during cortical malformation induced by neonatal freeze-lesion. *Neurosci Res* 59: 288–295, 2007.

Sloviter RS, Zappone CA, Harvey BD, Frotscher M. Kainic acid-induced recurrent mossy fiber innervation of dentate gyrus inhibitory interneurons: possible anatomical substrate of granule cell hyper-inhibition in chronically epileptic rats. *J Comp Neurol* 494: 944–960, 2006.

Sutula T, Cascino G, Cavazos J, Parada I, Ramirez L. Mossy fiber synaptic reorganization in the epileptic human temporal lobe. *Ann Neurol* 26: 321–330, 1989.

Taylor DC, Falconer MA, Bruton CJ, Corsellis JA. Focal dysplasia of the cerebral cortex in epilepsy. *J Neurol Neurosurg Psychiatry* 34: 369–387, 1971.

Thomson AM, Bannister AP. Interlaminar connections in the neocortex. *Cereb Cortex* 13: 5–14, 2003.

Uematsu M, Hirai Y, Karube F, Ebihara S, Kato M, Abe K, Obata K, Yoshida S, Hirabayashi M, Yanagawa Y, Kawaguchi Y. Quantitative chemical composition of cortical GABAergic neurons revealed in transgenic venus-expressing rats. *Cereb Cortex* 18: 315–330, 2008.

Wang T, Kumada T, Morishima T, Iwata S, Kaneko T, Yanagawa Y, Yoshida S, Fukuda A. Accumulation of GABAergic neurons, causing a focal ambient gaba gradient, and downregulation of KCC2 are induced during microgyrus formation in a mouse model of polymicrogyria. *Cereb Cortex* 24: 1088–1101, 2014.

Xiang Z, Huguenard JR, Prince DA. Synaptic inhibition of pyramidal cells evoked by different interneuronal subtypes in layer v of rat visual cortex. *J Neurophysiol* 88: 740–750, 2002.

Yang JM, Zhang J, Yu YQ, Duan S, Li XM. Postnatal development of 2 microcircuits involving fast-spiking interneurons in the mouse prefrontal cortex. *Cereb Cortex* 24: 98–109, 2014.

Zhou FW, Roper SN. Densities of glutamatergic and GABAergic presynaptic terminals are altered in experimental cortical dysplasia. *Epilepsia* 51: 1468–1476, 2010.

Zhu WJ, Roper SN. Reduced inhibition in an animal model of cortical dysplasia. *J Neurosci* 20: 8925–8931, 2000.

Zilles K, Qu M, Schleicher A, Luhmann HJ. Characterization of neuronal migration disorders in neocortical structures: quantitative receptor autoradiography of ionotropic glutamate, GABA(A) and GABA(B) receptors. *Eur J Neurosci* 10: 3095–3106, 1998.